INTERNATIONAL JOURNAL FOR NUMERICAL METHODS IN FLUIDS
Int. J. Numer. Meth. Fluids 2004; **46**:1181–1199
Published online in Wiley InterScience (www.interscience.wiley.com). DOI: 10.1002/fld.795

Fluid flow analysis by finite element method using arbitrarily deformed elements (Proposal of the GMSR-method)

Y. Matsuda*,†, C. Shao‡, M. Yoshino, M. Hoshihara§ and Y. Tanaka

Department of Mechanical Systems Engineering, Faculty of Engineering, Shinshu University, Nagano 380-8553, Japan

SUMMARY

The generalized MSR-method (GMSR-method) is proposed as a finite element fluid analysis algorithm for arbitrarily deformed elements using the error analysis approach. The MSR-method was originally developed by one of the authors in our previous research works using a modified Galerkin method (MGM) for a convection–diffusion equation and the SIMPLER-approach. In this paper, this MGM is developed theoretically in the case of arbitrarily deformed elements using the error analysis approach. In the GMSR-method, since the inertia term and the pressure term are considered explicitly, only symmetrical matrices appear. Hence, it helps us reduce computational memory and computation time. Moreover, artificial viscosity and diffusivity are introduced through an error analysis approach to improve the accuracy and stability. This GMSR-method is applied for two- and three-dimensional natural convection problems in a cavity. In the computations at different Rayleigh numbers, it is shown that this method gives reasonable results compared to other research works. Thus, it is found that the GMSR-method is applicable to thermal-fluid flow problems with complicated boundaries. Copyright © 2004 John Wiley & Sons, Ltd.

KEY WORDS: finite element method; arbitrarily deformed elements; error analysis approach; cavity flow; natural convection

1. INTRODUCTION

Thermal-fluid flow analyses in natural convection problems are subjects of much interest in many science and engineering fields. Recently, Matsuda *et al.* [1] have proposed a finite element method (the MSR-method) which is a combination of a modified Galerkin method (MGM) and the SIMPLE Revised (SIMPLER) algorithm [2]. The MGM was originally developed as an effective algorithm for a convection–diffusion equation. Comparing with a conventional Galerkin method, in the MGM, convection terms are considered explicitly, and only

*Correspondence to: Y. Matsuda, 4-17-1, Wakasato, Nagano City, Nagano 380-8553, Japan.
†E-mail: matsuda@gipwc.shinshu-u.ac.jp, ymatsuda@bolero.plala.or.jp, URL: http://www11.plala.or.jp/faw/
‡Present address: AW Engineering Co. Ltd., Anjo City, Aichi 444-1164, Japan.
§Present address: Rinnai Co. Ltd., Nagoya City, Aichi 454-0802, Japan.

Received 5 June 2003
Revised 9 April 2004

symmetrical matrices appear. In addition, an artificial diffusivity is introduced into the formulation through an error analysis approach to improve the accuracy and stability of the MGM [3, 4]. On the other hand, the SIMPLER algorithm is well known as one of the methods for solving coupled problems of the velocity and the pressure. The MSR-method is applied to a three-dimensional natural convection problem in a cubic cavity up to the Rayleigh number of 10^8 [5], and its effectiveness is verified compared to other studies. In their method, however, the shapes of the finite elements are confined to specific forms such as triangle, square, tetrahedron and cube. Therefore, it is required that a new method for any form of finite elements based on the error analysis approach should be developed in order to solve actual thermal-fluid flow problems with complicated boundaries.

In this paper, we propose the generalized MSR-method (GMSR-method) for arbitrarily deformed elements using the error analysis approach, and investigate its effectiveness in two- and three-dimensional benchmark problems.

2. METHOD OF COMPUTATION

2.1. The 'GMSR' algorithm

The GMSR-method is based on the 'generalized' MGM for arbitrarily deformed elements and the SIMPLER-approach. Then, this method is verified through its application for the thermal-fluid analyses problems. An incompressible viscous fluid flow with heat transfer is considered.

The Boussinesq approximation is used for the gravitational term and the buoyancy force is assumed to be acting in the x_2-direction alone. Then, the governing equations in the non-dimensional form are expressed as follows:

$$\nabla \cdot \mathbf{u} = 0 \tag{1}$$

$$\frac{\partial \mathbf{u}}{\partial t} + \mathbf{u} \cdot \nabla \mathbf{u} = -\nabla p + Pr\, \nabla^2 \mathbf{u} + Ra\, Pr\, \theta \mathbf{j} \tag{2}$$

$$\frac{\partial \theta}{\partial t} + \mathbf{u} \cdot \nabla \theta = \nabla^2 \theta \tag{3}$$

where t is the time, $\mathbf{u}$ is the fluid velocity, p is the pressure, θ is the fluid temperature, $\mathbf{j}$ is the unit vector in the x_2-direction opposite to the gravitational force, and the dimensionless parameters Pr and Ra are Prandtl and Rayleigh numbers, respectively.

The first step of the MSR algorithm is the derivation of the approximate pressure p^*. Equation (2) is discretized in the temporal direction using the forward Euler method as follows:

$$\frac{\mathbf{u}^{n+1} - \mathbf{u}^n}{\Delta t} + \mathbf{u}^n \cdot \nabla \mathbf{u}^n = -\nabla p^* + Pr\, \nabla^2 \mathbf{u}^n + Ra\, Pr\, \theta^n \mathbf{j} \tag{4}$$

where Δt is the time step, p^* is an approximation of p^{n+1}, and the superscript n indicates the value at $t = n\Delta t$. Equation (4) is divided into the following two equations:

$$\hat{\mathbf{u}} = \mathbf{u}^n + \Delta t \{ Pr\, \nabla^2 \mathbf{u}^n + Ra\, Pr\, \theta^n \mathbf{j} - \mathbf{u}^n \cdot \nabla \mathbf{u}^n \} \tag{5}$$

$$\mathbf{u}^{n+1} = \hat{\mathbf{u}} - \Delta t \nabla p^* \tag{6}$$

where $\hat{\mathbf{u}}$ is generally called a pseudo-velocity. Taking a divergence of Equation (6) and considering Equation (1) for $\mathbf{u}^{n+1}$, we get the following Poisson equation for p^*:

$$\nabla^2 p^* = \frac{\nabla \cdot \hat{\mathbf{u}}^n}{\Delta t} \tag{7}$$

The approximate pressure p^* is obtained using the conventional Galerkin finite element method.

The second step is the computations of the approximate velocity $\mathbf{u}^*$ and of a new temperature θ^{n+1}. Using the calculated pressure p^*, Equations (2) and (3) are solved by the following procedure. These two equations are discretized by the conventional Galerkin finite element method. Here the temporal differential term is approximated as follows:

$$\phi \left(\frac{\partial \mathbf{u}}{\partial t}\right)^* + (1-\phi)\left(\frac{\partial \mathbf{u}}{\partial t}\right)^n = \frac{\mathbf{u}^* - \mathbf{u}^n}{\Delta t} \tag{8}$$

$$\phi \left(\frac{\partial \theta}{\partial t}\right)^{n+1} + (1-\phi)\left(\frac{\partial \theta}{\partial t}\right)^n = \frac{\theta^{n+1} - \theta^n}{\Delta t} \tag{9}$$

where ϕ is a time scheme parameter. It should be noted that the inertia, the pressure and the gravitational terms are dealt with explicitly. Thus we obtain the following finite element equations:

$$\left\{\frac{[P]}{\Delta t} + \phi[D]_u\right\}\{\mathbf{u}_\gamma\}^* = \left\{\frac{[P]}{\Delta t} - (1-\phi)[D]_u\right\}\{\mathbf{u}_\gamma\}^n - \{F_\gamma\}_u^n \tag{10}$$

$$\left\{\frac{[P]}{\Delta t} + \phi[D]_\theta\right\}\{\theta\}^{n+1} = \left\{\frac{[P]}{\Delta t} - (1-\phi)[D]_\theta\right\}\{\theta\}^n - \{F\}_\theta^n \tag{11}$$

where $\mathbf{u}_\gamma$ $(\gamma = 1,2,3)$ is the component of velocity vector $\mathbf{u}$, and $\{\mathbf{u}_\gamma\}$ and $\{\theta\}$ are vectors whose element is the value of the variable at each node. In the Cartesian co-ordinates, we get:

$$[P] = \sum_{e=1}^{M} \int_{V_e} N_i N_j \, \mathrm{d}x_1 \, \mathrm{d}x_2 \, \mathrm{d}x_3 \tag{12a}$$

$$[D]_u = \sum_{e=1}^{M} \int_{V_e} f_u \, Pr \, \frac{\partial N_i}{\partial x_\delta} \frac{\partial N_j}{\partial x_\delta} \, \mathrm{d}x_1 \, \mathrm{d}x_2 \, \mathrm{d}x_3 \tag{12b}$$

$$[D]_\theta = \sum_{e=1}^{M} \int_{V_e} f_\theta \, \frac{\partial N_i}{\partial x_\delta} \frac{\partial N_j}{\partial x_\delta} \, \mathrm{d}x_1 \, \mathrm{d}x_2 \, \mathrm{d}x_3 \tag{12c}$$

$$\{F_\gamma\}_u^n = \sum_{e=1}^{M} \int_{V_e} N_i \left(\mathbf{u}_\delta^n \frac{\partial \mathbf{u}_\gamma^n}{\partial x_\delta} + \frac{\partial p^*}{\partial x_\gamma} - Ra \, Pr \, \theta^n \delta_{\gamma 2}\right) \mathrm{d}x_1 \, \mathrm{d}x_2 \, \mathrm{d}x_3 \tag{12d}$$

$$\{F\}_\theta^n = \sum_{e=1}^{M} \int_{V_e} N_i \mathbf{u}_\delta^n \frac{\partial \theta^n}{\partial x_\delta} \, \mathrm{d}x_1 \, \mathrm{d}x_2 \, \mathrm{d}x_3 \tag{12e}$$

where V_e is the domain of an element, N_i is a shape function, M is the total number of elements, δ_{γ^2} is the Kronecker delta, and f_u and f_θ are correction coefficients for the viscosity term and for the diffusion term, respectively. Note that (x_1, x_2, x_3) represents Cartesian co-ordinates and the summation convention is used for the subscript δ ($\delta = 1, 2, 3$). The above correction coefficients f_u and f_θ are introduced to improve the numerical accuracy and stability, and these values are determined through an error analysis approach. The formulations of Equations (10) and (11) are referred as the MGM. Since the coefficient matrices appearing in the left-hand side of Equations (10) and (11) are symmetrical in the MGM, we obtain less memory size and shorter computation time than conventional Galerkin methods.

The third step is the derivation of the corrected quantity of the pressure. Once the approximate velocity $\mathbf{u}^*$ is obtained, the new velocity $\mathbf{u}^{n+1}$ is given as follows. Considering Equation (2) for the velocities $\mathbf{u}^*$ and $\mathbf{u}^{n+1}$, we get

$$\frac{\mathbf{u}^* - \mathbf{u}^n}{\Delta t} + \mathbf{u}^* \cdot \nabla \mathbf{u}^* = -\nabla p^* + Pr\,\nabla^2 \mathbf{u}^* + Ra\,Pr\,\theta^* \mathbf{j} \tag{13}$$

$$\frac{\mathbf{u}^{n+1} - \mathbf{u}^n}{\Delta t} + \mathbf{u}^{n+1} \cdot \nabla \mathbf{u}^{n+1} = -\nabla p^{n+1} + Pr\,\nabla^2 \mathbf{u}^{n+1} + Ra\,Pr\,\theta^{n+1} \mathbf{j} \tag{14}$$

It is assumed that the convection, the viscosity and the gravitational terms can be negligible because these effects are taken into account in Equation (11). Hence, subtracting Equation (13) from Equation (14), we obtain the following Poisson equation:

$$\frac{\mathbf{u}^{n+1} - \mathbf{u}^*}{\Delta t} = -\nabla(\delta p) \tag{15}$$

where

$$\delta p = p^{n+1} - p^* \tag{16}$$

Taking the divergence of Equation (15), we have the following Poisson equation:

$$\nabla^2(\delta p) = \frac{\nabla \cdot \mathbf{u}^*}{\Delta t} \tag{17}$$

The above equation is also computed using the conventional Galerkin method.

The final step is the corrections of the velocity and the pressure. Using the δp obtained by solving Equation (17), the new velocity $\mathbf{u}^{n+1}$ and pressure p^{n+1} are corrected as follows:

$$\mathbf{u}^{n+1} = \mathbf{u}^* - \Delta t \nabla(\delta p) \tag{18}$$

$$p^{n+1} = p^* + \delta p \tag{19}$$

The above procedure to obtain the new velocity and pressure is the same as the SIMPLER procedure. However, we obtain an approximate velocity $\mathbf{u}^*$ and a new temperature θ^{n+1} by means of the MGM for Equations (10) and (11). We call these coupling procedures the MSR method in this paper.

2.2. Transformation into generalized co-ordinates

We consider a linear arbitrarily deformed hexahedral element with eight nodes, as shown in Figure 1. Applying the transformation from Cartesian to generalized co-ordinates, the hexahe-

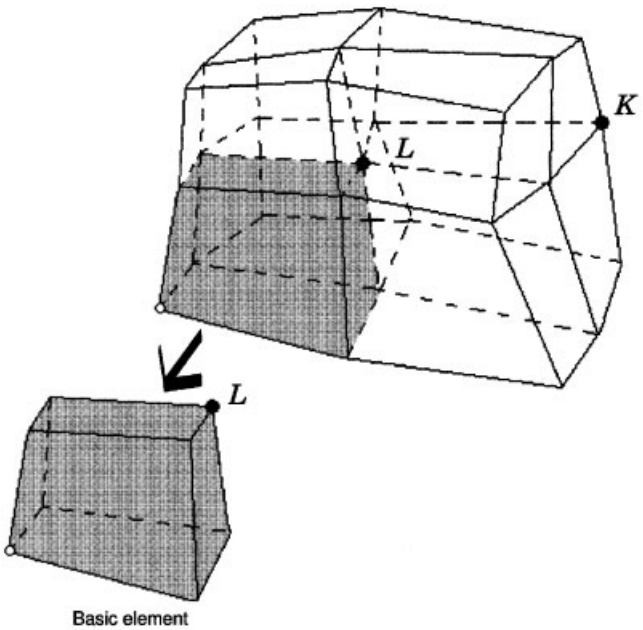

Figure 1. Nodes in linear arbitrarily deformed hexahedral element: a node 'L' is set to the origin and the co-ordinates of the surrounding nodes including 'L' are defined as 'K' $(a_{1K}h_1, a_{2K}h_2, a_{3K}h_3)$, where h_γ $(\gamma = 1,2,3)$ is a typical mesh size in the x_γ-direction.

dron is transformed into a cube in the new co-ordinates. We now define the spatial variation of the physical variable ω $(= \mathbf{u}_\gamma, \theta)$ over the element by

$$\omega = \sum_{i=1}^{8} N_i(\xi_1, \xi_2, \xi_3)\omega_i \tag{20}$$

where ω_i means the value at the node i. The shape functions in this case are given by

$$N_i(\xi_1, \xi_2, \xi_3) = \tfrac{1}{8}(1 + E_{1i}\xi_1)(1 + E_{2i}\xi_2)(1 + E_{3i}\xi_3) \quad \text{for } i = 1,2,K,8 \tag{21}$$

with $[E_{1i}, E_{2i}, E_{3i}] = [\pm 1, \pm 1, \pm 1]$.

In order to compute the finite element equations, the transformation for the first derivative is needed. According to the chain rule of the partial differentiation, we obtain the following relations:

$$\begin{Bmatrix} \dfrac{\partial}{\partial \xi_1} \\ \dfrac{\partial}{\partial \xi_2} \\ \dfrac{\partial}{\partial \xi_3} \end{Bmatrix} = [J] \begin{Bmatrix} \dfrac{\partial}{\partial x_1} \\ \dfrac{\partial}{\partial x_2} \\ \dfrac{\partial}{\partial x_3} \end{Bmatrix} \tag{22}$$

where $[J]$ is the Jacobian with respect to the transformation and given by

$$[J]=\begin{bmatrix} \dfrac{\partial x_1}{\partial \xi_1} & \dfrac{\partial x_2}{\partial \xi_1} & \dfrac{\partial x_3}{\partial \xi_1} \\ \dfrac{\partial x_1}{\partial \xi_2} & \dfrac{\partial x_2}{\partial \xi_2} & \dfrac{\partial x_3}{\partial \xi_2} \\ \dfrac{\partial x_1}{\partial \xi_3} & \dfrac{\partial x_2}{\partial \xi_3} & \dfrac{\partial x_3}{\partial \xi_3} \end{bmatrix} = \begin{bmatrix} \displaystyle\sum_{i=1}^{8} \frac{\partial N_i}{\partial \xi_1} x_{1i} & \displaystyle\sum_{i=1}^{8} \frac{\partial N_i}{\partial \xi_1} x_{2i} & \displaystyle\sum_{i=1}^{8} \frac{\partial N_i}{\partial \xi_1} x_{3i} \\ \displaystyle\sum_{i=1}^{8} \frac{\partial N_i}{\partial \xi_2} x_{1i} & \displaystyle\sum_{i=1}^{8} \frac{\partial N_i}{\partial \xi_2} x_{2i} & \displaystyle\sum_{i=1}^{8} \frac{\partial N_i}{\partial \xi_2} x_{3i} \\ \displaystyle\sum_{i=1}^{8} \frac{\partial N_i}{\partial \xi_3} x_{1i} & \displaystyle\sum_{i=1}^{8} \frac{\partial N_i}{\partial \xi_3} x_{2i} & \displaystyle\sum_{i=1}^{8} \frac{\partial N_i}{\partial \xi_3} x_{3i} \end{bmatrix} \tag{23}$$

Thus, taking the inverse of the matrix $[J]$, we get the following expression:

$$\begin{Bmatrix} \dfrac{\partial}{\partial x_1} \\ \dfrac{\partial}{\partial x_2} \\ \dfrac{\partial}{\partial x_3} \end{Bmatrix} = [J]^{-1} \begin{Bmatrix} \dfrac{\partial}{\partial \xi_1} \\ \dfrac{\partial}{\partial \xi_2} \\ \dfrac{\partial}{\partial \xi_3} \end{Bmatrix} = \frac{\mathrm{adj}[J]}{\det[J]} \begin{Bmatrix} \dfrac{\partial}{\partial \xi_1} \\ \dfrac{\partial}{\partial \xi_2} \\ \dfrac{\partial}{\partial \xi_3} \end{Bmatrix} \tag{24}$$

where adj$[J]$ and det$[J]$ are the adjoint matrix and the determinant of $[J]$, respectively. Using these relations, Equation (12) can be rewritten as follows:

$$[P] = \sum_{e=1}^{M} \left[\int_{-1}^{1}\int_{-1}^{1}\int_{-1}^{1} N_i N_j \det[J]\, \mathrm{d}\xi_1\, \mathrm{d}\xi_2\, \mathrm{d}\xi_3 \right]_{V_e} \tag{25a}$$

$$[D]_u = \sum_{e=1}^{M} \left[\int_{-1}^{1}\int_{-1}^{1}\int_{-1}^{1} \frac{f_u Pr}{\det[J]} \left(\tilde{J}_{\zeta\delta} \frac{\partial N_i}{\partial \xi_\delta} \right) \left(\tilde{J}_{\zeta\varepsilon} \frac{\partial N_j}{\partial \xi_\varepsilon} \right) \mathrm{d}\xi_1\, \mathrm{d}\xi_2\, \mathrm{d}\xi_3 \right]_{V_e} \tag{25b}$$

$$[D]_\theta = \sum_{e=1}^{M} \left[\int_{-1}^{1}\int_{-1}^{1}\int_{-1}^{1} \frac{f_\theta}{\det[J]} \left(\tilde{J}_{\zeta\delta} \frac{\partial N_i}{\partial \xi_\delta} \right) \left(\tilde{J}_{\zeta\varepsilon} \frac{\partial N_j}{\partial \xi_\varepsilon} \right) \mathrm{d}\xi_1\, \mathrm{d}\xi_2\, \mathrm{d}\xi_3 \right]_{V_e} \tag{25c}$$

$$\{F_\gamma\}_u^n = \sum_{e=1}^{M} \left[\int_{-1}^{1}\int_{-1}^{1}\int_{-1}^{1} N_i \left(u_\varepsilon^n \tilde{J}_{\varepsilon\delta} \frac{\partial u_\gamma^n}{\partial \xi_\delta} + \tilde{J}_{\gamma\delta} \frac{\partial p^*}{\partial \xi_\delta} - Ra\, Pr\, \theta^n \det[J] \delta_{\gamma_2} \right) \mathrm{d}\xi_1\, \mathrm{d}\xi_2\, \mathrm{d}\xi_3 \right]_{V_e} \tag{25d}$$

$$\{F\}_\theta^n = \sum_{e=1}^{M} \left[\int_{-1}^{1}\int_{-1}^{1}\int_{-1}^{1} N_i u_\varepsilon^n \tilde{J}_{\varepsilon\delta} \frac{\partial \theta^n}{\partial \xi_\delta} \mathrm{d}\xi_1\, \mathrm{d}\xi_2\, \mathrm{d}\xi_3 \right]_{V_e} \tag{25e}$$

where $\tilde{J}_{\varepsilon\delta}$ is the element of the adj$[J]$, and the summation convention is used for the subscript δ, ε and ς $(\delta, \varepsilon, \varsigma = 1, 2, 3)$ hereafter. The numerical integration can be calculated by using the Gaussian quadrature. For a general function $F(\xi_1, \xi_2, \xi_3)$, the Gaussian quadrature leads to an equation of the following form:

$$\int_{-1}^{1}\int_{-1}^{1}\int_{-1}^{1} F(\xi_1, \xi_2, \xi_3) \det[J]\, \mathrm{d}\xi_1\, \mathrm{d}\xi_2\, \mathrm{d}\xi_3 = \sum_{i=1}^{l}\sum_{j=1}^{l}\sum_{k=1}^{l} W_i \cdot W_j \cdot W_k F(\xi_{1i}^*, \xi_{2j}^*, \xi_{3k}^*) \tag{26}$$

where l is the total number of the Gaussian integration points $(\xi^*_{1i}, \xi^*_{2j}, \xi^*_{3k})$, and W_i, W_j and W_k are weighting factors corresponding to each Gaussian point. In the following computations, the value of l is set to 2, in which $W_i = W_j = W_k = 1$ and the co-ordinates of the Gaussian points are $(\xi^*_{1i}, \xi^*_{2J}, \xi^*_{3k}) = (\pm 1/\sqrt{3}, \pm 1/\sqrt{3}, \pm 1/\sqrt{3})$.

2.3. The 'generalized' MGM through an error analysis approach

The correction coefficients f_u and f_θ that are introduced in Equations (12) and (25) are regarded as artificial viscosity and diffusivity, respectively. They are determined through the error analysis approach, which is based on a general solution for a convection–diffusion equation. In the following, Equation (2) is taken as an example to explain the derivation of the coefficients, but the same method can be applied to Equation (3) for the temperature. In this approach, it is assumed that Equation (2) is a convection–diffusion equation by neglecting the pressure term and the gravitational term and by linearizing the inertia term. Moreover, multiplying the viscosity term and the inertia term by f_u and g_u, respectively, we obtain

$$\frac{\partial u_\gamma}{\partial t} + g_u U_\delta \frac{\partial u_\gamma}{\partial x_\delta} = f_u Pr \frac{\partial^2 u_\gamma}{\partial x_\delta^2} \tag{27}$$

where U_δ is assumed a constant value. Here, setting the co-ordinates of a node 'L' to $(\alpha_{1L} h_1, \alpha_{2L} h_2, \alpha_{3L} h_3)$, where h_γ $(\gamma = 1, 2, 3)$ is a typical mesh size, the amplification factor ζ_A of a general solution in Equation (27) is expressed as follows [5]:

$$\zeta_A = R_1 + IR_2 \tag{28}$$

with

$$R_1 = \exp[-(\beta_\delta h_\delta)^2 r_\delta] \cos(b_\delta \beta_\delta h_\delta) \tag{29a}$$

$$R_2 = -\exp[-(\beta_\delta h_\delta)^2 r_\delta] \sin(b_\delta \beta_\delta h_\delta) \tag{29b}$$

where $I = \sqrt{-1}$ is the imaginary unit, $\beta_\delta = (-\infty, \infty)$ is a wave number in the x_δ-direction, and the dimensionless parameters $b_\gamma = U_\gamma \Delta t / h_\gamma$ and $r_\gamma = Pr\, \Delta t / h_\gamma^2$ are the Courant and Fourier numbers, respectively. On the other hand, the amplification factor ζ_N of a numerical solution in Equation (27) can be written as follows:

$$\zeta_N = \frac{Q_1 + f_u Q_2 + g_u Q_3 + I(Q_4 + f_u Q_5 + g_u Q_6)}{Q_1 + f_u Q_7 + I(Q_4 + f_u Q_8)} \tag{30}$$

where Q_i $(i = 1, 2, K, 8)$ multiplied by 1, f_u and g_u are derived from the unsteady, the viscosity and the inertia terms, respectively. Here, as shown in Figure 1, we set the node 'L' to the origin and define the co-ordinates of the surrounding nodes including 'L' as 'K' $(\alpha_{1K} h_1, \alpha_{2K} h_2, \alpha_{3K} h_3)$ for $K = 1, 2, K, 27$. In such a case, the expressions of Q_i are given in Appendix A.

The two coefficients f_u and g_u are determined by equating the real and imaginary parts of ζ_N with those of ζ_A under the limits of $\beta_\gamma h_\gamma \to 0$ for all $\gamma = 1, 2, 3$. Since $\beta_\gamma h_\gamma = 2\pi h_\gamma / \lambda_\gamma$ (where λ_γ is the wave length in the x_γ-direction), these limits mean that very fine meshes

are used in the computations. From Equations (28) and (30), we obtain

$$f_u = \lim_{\beta_\gamma h_\gamma \to 0} \frac{Q_3 S_1 - Q_6 S_2}{Q_6 S_3 - Q_3 S_4} \tag{31}$$

$$g_u = \lim_{\beta_\gamma h_\gamma \to 0} \frac{S_2 S_4 - S_1 S_3}{Q_6 S_3 - Q_3 S_4} \tag{32}$$

with

$$S_1 = Q_4(1 - R_1) - R_2 Q_1 \tag{33a}$$

$$S_2 = Q_1(1 - R_1) + R_2 Q_4 \tag{33b}$$

$$S_3 = Q_2 - R_1 Q_7 + R_2 Q_8 \tag{33c}$$

$$S_4 = Q_5 - R_1 Q_8 - R_2 Q_7 \tag{33d}$$

Notice that the L'Hospital theorem is used in the calculations of the limit values. Performing the differentiations of the numerators and denominators in Equations (31) and (32), we get the following expressions independent of the wave numbers:

$$f_u = \lim_{\beta_\gamma h_\gamma \to 0} \frac{-Q_3'' R_2' Q_1 - Q_6'(-Q_1 R_1'' + 2R_2' Q_4)}{Q_6'(Q_2'' - Q_7'')} \tag{34}$$

$$g_u = \lim_{\beta_\gamma h_\gamma \to 0} \frac{R_2' Q_1}{Q_6'} \tag{35}$$

Substituting the limit values given in Appendix B into Equations (34) and (35), we finally obtain the coefficients f_u and g_u:

$$f_u = -\frac{A^{(0)}(b_1 + b_2 + b_3)(C_1^{(2)} b_1 + C_2^{(2)} b_2 + C_3^{(2)} b_3)}{(C_1^{(1)} b_1 + C_2^{(1)} b_2 + C_3^{(1)} b_3)(B_1^{(2)} r_1 + B_2^{(2)} r_2 + B_3^{(2)} r_3)} + \frac{A^{(0)}\{2(r_1 + r_2 + r_3) + (b_1 + b_2 + b_3)^2\} - 2A^{(1)}(b_1 + b_2 + b_3)}{B_1^{(2)} r_1 + B_2^{(2)} r_2 + B_3^{(2)} r_3} \tag{36}$$

$$g_u = -\frac{A^{(0)}(b_1 + b_2 + b_3)}{C_1^{(1)} b_1 + C_2^{(1)} b_2 + C_3^{(1)} b_3} \tag{37}$$

with

$$A^{(0)} = \sum_{K=1}^{27} P_K \tag{38a}$$

$$A^{(1)} = \sum_{K=1}^{27} P_K(\alpha_{1K} + \alpha_{2K} + \alpha_{3K}) \tag{38b}$$

$$B_\gamma^{(2)} = \sum_{K=1}^{27} \left[-D_{\gamma,K}(\alpha_{1K} + \alpha_{2K} + \alpha_{3K})^2\right] \tag{38c}$$

$$C_\gamma^{(1)} = \sum_{K=1}^{27} F_{\gamma,K}(\alpha_{1K} + \alpha_{2K} + \alpha_{3K}) \tag{38d}$$

$$C_\gamma^{(2)} = -\sum_{K=1}^{27} \left[F_{\gamma,K}(\alpha_{1K} + \alpha_{2K} + \alpha_{3K})^2\right] \tag{38e}$$

where P_K, $D_{\gamma,K}$ and $F_{\gamma,K}$ are given in Appendix A. In particular, the correction coefficients in a linear non-uniform cuboidal element are specified as follows:

$$f_u = 1 + \frac{(b_1 + b_2 + b_3)^2}{2(r_1 + r_2 + r_3)} + \frac{(\sigma_1 - 1)b_1 + (\sigma_2 - 1)b_2 + (\sigma_3 - 1)b_3}{6(r_1 + r_2 + r_3)} \tag{39}$$

$$g_u = 1 \tag{40}$$

where σ_γ ($\gamma = 1,2,3$) is the ratio of mesh size in the x_γ-direction.

For the temperature θ in Equation (3), on the other hand, the correction coefficients f_θ and g_θ are obtained in the same form as Equations (36) and (37) except that the Fourier number in Equation (3) is given by $r_\gamma = \Delta t/h_\gamma^2$.

3. NUMERICAL RESULTS

3.1. Natural convection problems in a square cavity

In order to check the validity of the proposed method, we first compute the buoyancy-driven flows in a two-dimensional square cavity of 1×1, as shown in Figure 2, using the MSR method. The initial conditions are $\mathbf{u} = 0$ and $\theta = 0$ in the whole domain. The boundary conditions are imposed as follows: $\mathbf{u} = 0$ and $(\partial p/\partial n) = 0$ at all walls, $\theta = 1$ and $\theta = 0$ at the left-

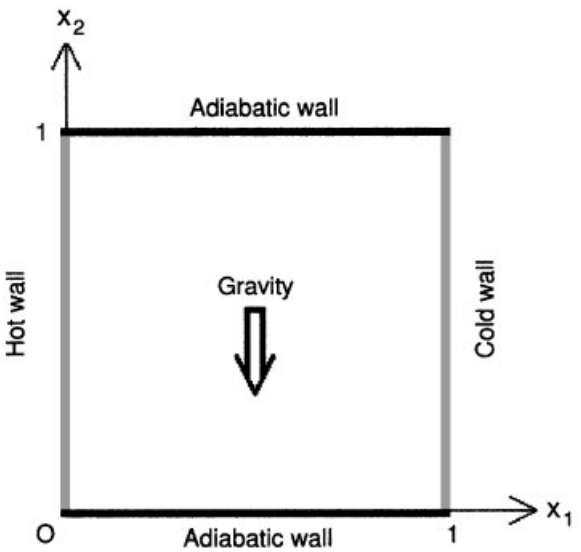

Figure 2. Geometry of two-dimensional natural convection problem.

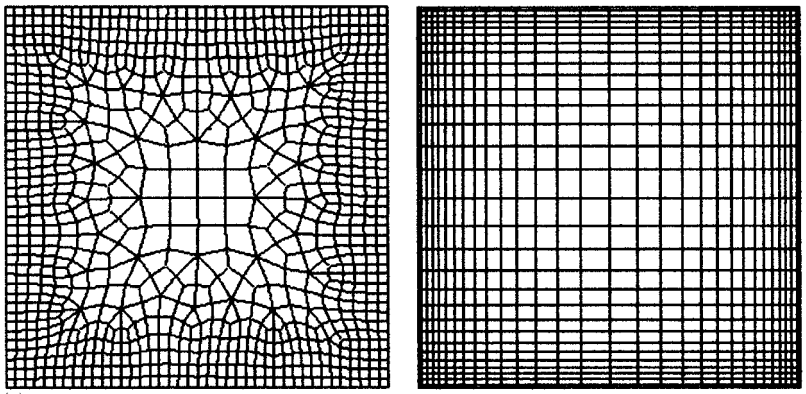

Figure 3. Mesh configurations: (a) arbitrary quadrilateral mesh; and (b) non-uniform rectangular mesh.

and right-hand sides of walls, respectively, and $(\partial\theta/\partial n)=0$ at the other walls, where $\partial/\partial n=0$ is the derivative normal to the boundary. The Prandtl number Pr is kept at 0.71, and the Rayleigh number Ra is set to 710 and 10^5. The computations are carried out by using two types of mesh configurations: one is an arbitrary quadrilateral mesh and the other is a non-uniform rectangular mesh, as shown in Figure 3. The steady state criterion δ is defined as follows:

$$\delta=\max\left\{\left|\frac{u_1^m-u_1^{m-1}}{u_1^m}\right|,\left|\frac{u_2^m-u_2^{m-1}}{u_2^m}\right|\right\}\times 100\leqslant 0.001\ (\%)$$
$$\text{for } \forall|u_1^m|,|u_2^m|\geqslant\max\{|u_1^{m-1}|,|u_2^{m-1}|\}\times 0.001 \tag{41}$$

To examine the actual heat flux across the cavity, the average Nusselt number $\overline{Nu}_0$ on the hot wall is calculated by

$$\overline{Nu}_0=\int_0^1\left|\frac{\partial\theta}{\partial x_1}\right|_{x_1=0}\mathrm{d}x_2 \tag{42}$$

where $|\cdot|$ means the absolute value. The average Nusselt number $\overline{Nu}_1$ on the cold wall is defined in the same way. In the above equation, the first derivative of the temperature is discretized by the one-sided second-order difference approximation and the integral is numerically calculated by the Simpson formula.

Table I presents the computational parameters and the numerical results. In this table, $u_{1,\max}$ and $u_{2,\max}$ are the maximum velocities in the x_1- and x_2-directions, respectively. It should be noted that the number of meshes are determined so that the number of nodes are almost equal in the two mesh configurations.

Figure 4 shows the computed velocity vectors and isotherms at $Ra=10^5$ by using the two types of grid and Figure 5 shows the convergence history of the average Nusselt numbers on the hot and cold walls at $Ra=10^5$. It is found that these average Nusselt numbers reach

Table I. Computational parameters and numerical results in two-dimensional natural convection problem: (a) arbitrary quadrilateral element; (b) non-uniform rectangular element.

Ra	Element	Meshes	Nodes	Δt	Number of iterations	$u_{1,\max}$	$u_{2,\max}$	$\overline{Nu}_0$
10^5	(a)	888	969	1×10^{-4}	3234	36.04	68.59	4.703
	(b)	900	961	1×10^{-4}	3242	35.18	68.77	4.549

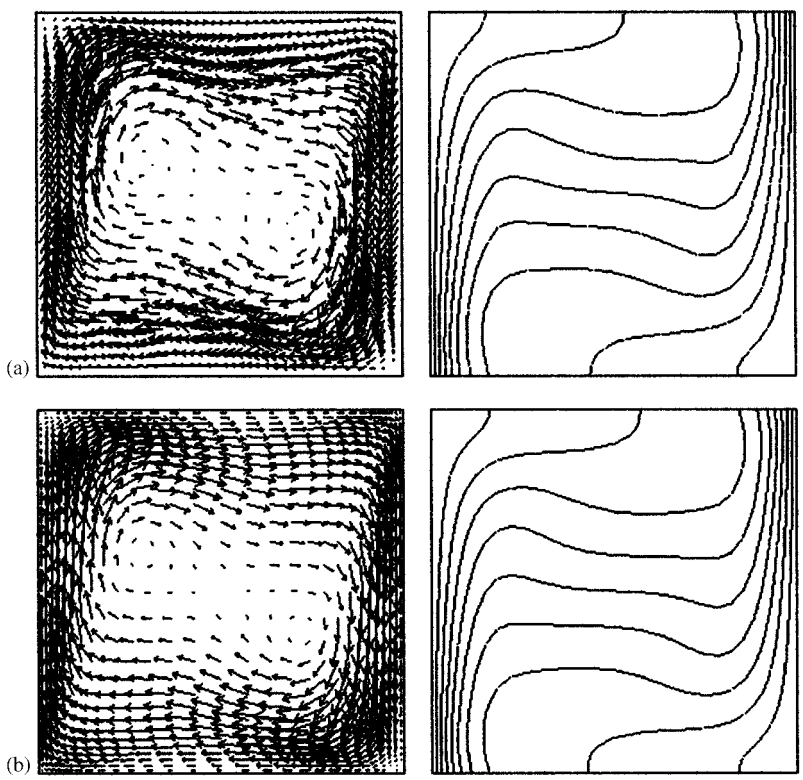

Figure 4. Computed velocity vectors (left) and isotherms (right) at $Ra = 10^5$ in two-dimensional natural convection problem: (a) arbitrary quadrilateral mesh; and (b) non-uniform rectangular mesh. (The contour interval of the isotherms is 0.1.)

almost the same value at the final state. Also, the present computations give reasonable results compared to those by Hortmann *et al.* [6]. Thus, it is found that the present method is valid for the thermal-fluid flow problems.

3.2. Natural convection problems in a cubic cavity

We next investigate the buoyancy-driven flows in a cubic cavity of $1 \times 1 \times 1$, as shown in Figure 6. The initial and boundary conditions are the same as in the previous two-dimensional problems. The Prandtl number Pr is 0.71, and the Rayleigh number Ra is set to 10^8. In the computations, we use a linear non-uniform cubic mesh of $50 \times 50 \times 50$ shown in Figure 7.

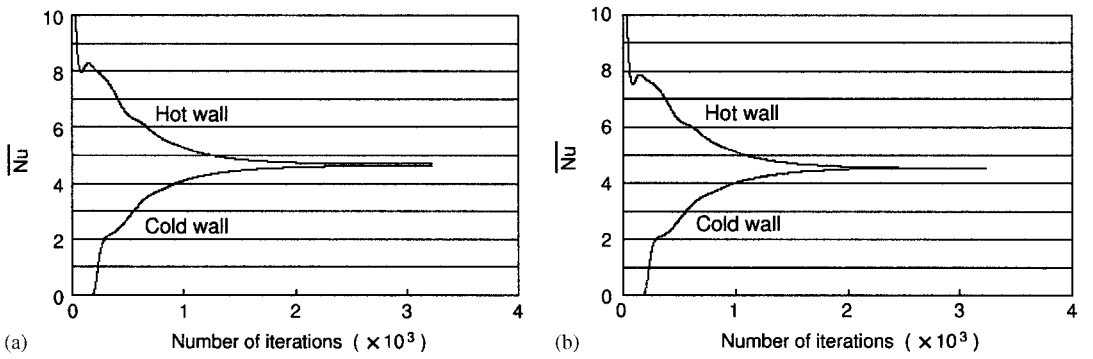

Figure 5. Convergence history of average Nusselt numbers at $Ra = 10^5$ in two-dimensional natural convection problem: (a) arbitrary quadrilateral mesh; and (b) non-uniform rectangular mesh.

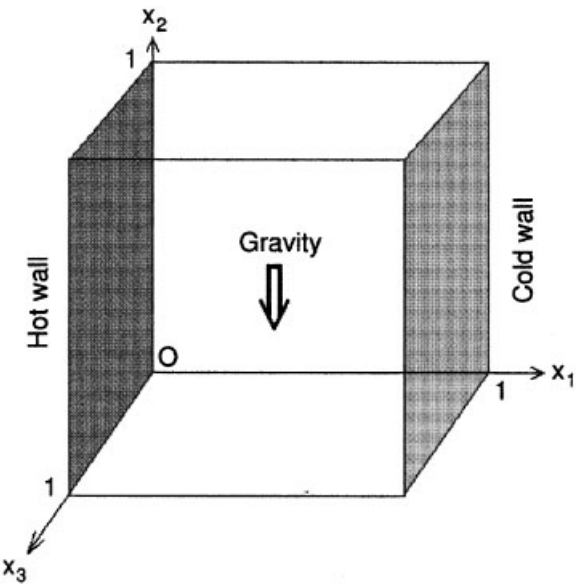

Figure 6. Geometry of three-dimensional natural convection problem.

The non-uniform mesh sizes are determined by the following equations [7]:

$$x_{\gamma i} = \begin{cases} \dfrac{\exp[a(i-1)\,\mathrm{d}x_\gamma] - 1}{2[\exp(a) - 1]} & \text{for } x_\gamma \leqslant 0.5 \\ \dfrac{\exp\{a[1-(i-1)]\,\mathrm{d}x_\gamma\} - 1}{2[\exp(a) - 1]} & \text{for } x_\gamma > 0.5 \end{cases} \tag{43}$$

with $a = 2$ and $\mathrm{d}x_\gamma = 2/(N_\gamma - 1)$, where N_γ denotes the number of grids in the x_γ-direction.

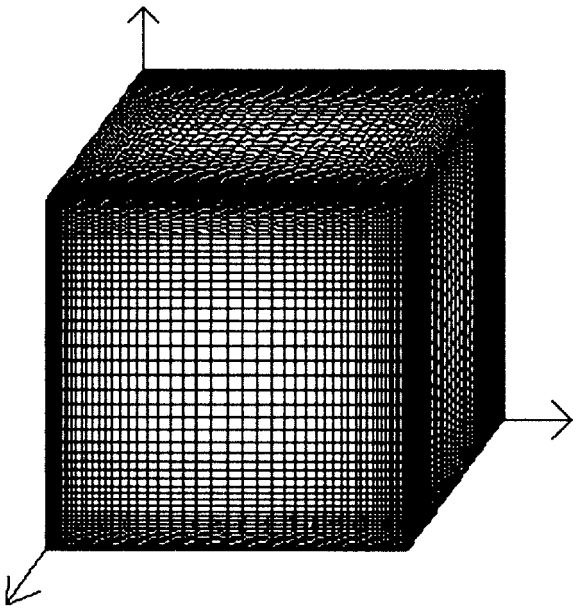

Figure 7. Non-uniform cuboidal mesh ($50 \times 50 \times 50$).

Table II. Computational parameters and numerical results in three-dimensional natural convection problem using non-uniform cuboidal element.

Ra	Element	Meshes	Δt	Number of iterations	$\overline{Nu}_0$
10^8	Non-uniform cuboid	$50 \times 50 \times 50$	1×10^{-6}	64 000	28.47

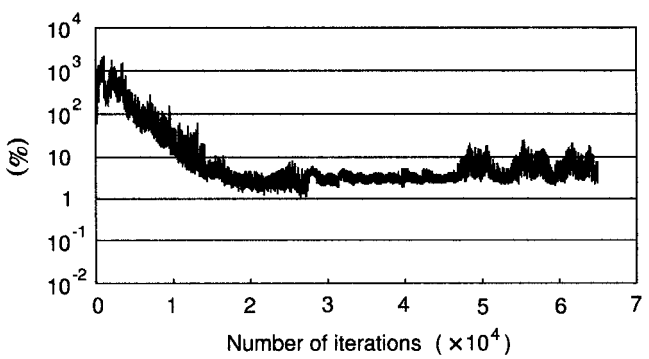

Figure 8. Time variation of δ in three-dimensional natural convection problem.

Table II presents the computational parameters and the numerical results. It should be noted that the number of iterations in this problem is a given value due to the unsteady flows described below. Figure 8 shows the time variation of δ. It is found that the value of δ remains around 10% and the steady-state criterion in Equation (41) is not satisfied in

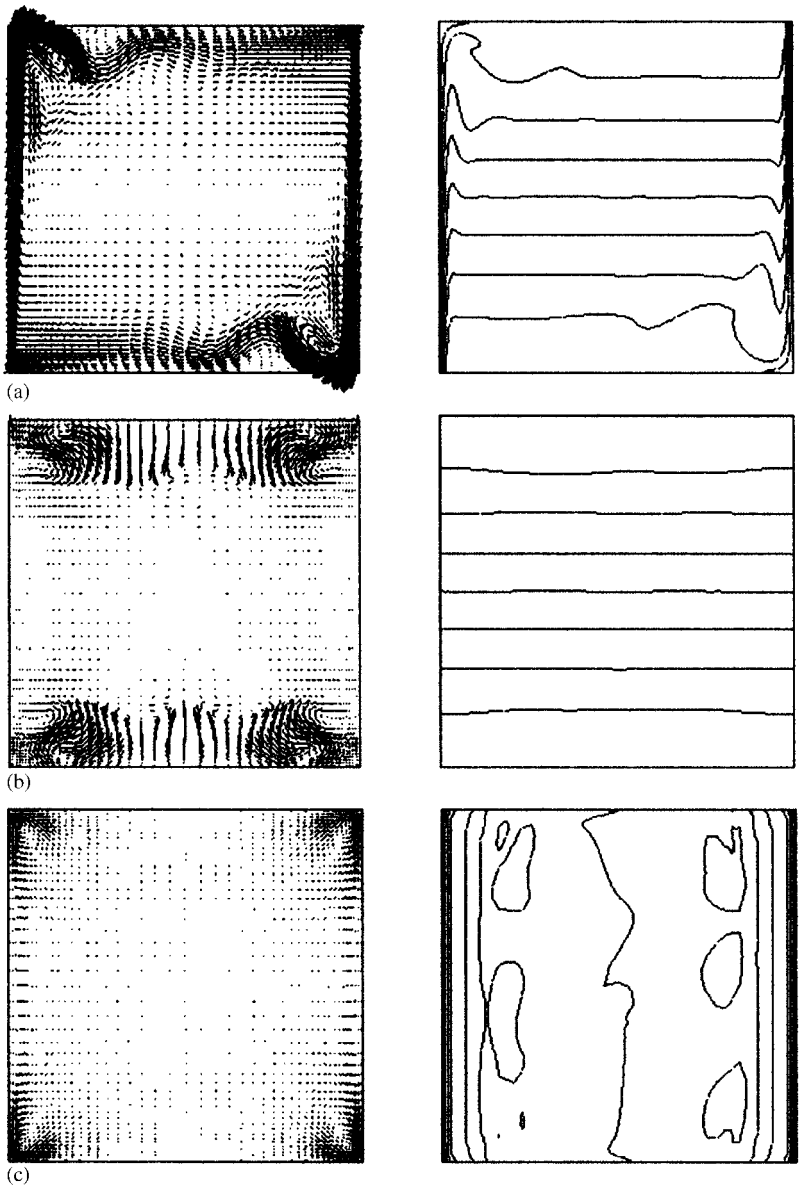

Figure 9. Computed velocity vectors (left) and isotherms (right) at $Ra = 10^8$ in three-dimensional natural convection problem: (a) x_1–x_2 plane at $x_3 = 0.5$; (b) x_2–x_3 plane at $x_1 = 0.5$; and (c) x_3–x_1 plane at $x_2 = 0.5$. (The contour interval of the isotherms is 0.1.)

this case. The reason would be that the flow becomes weak turbulent because there is strong buoyancy.

Figure 9 shows the computed velocity vectors and the isotherms after transitional flows, on the x_1–x_2 plane at $x_3 = 0.5$, x_2–x_3 plane at $x_1 = 0.5$ and x_3–x_1 plane at $x_2 = 0.5$. Note that

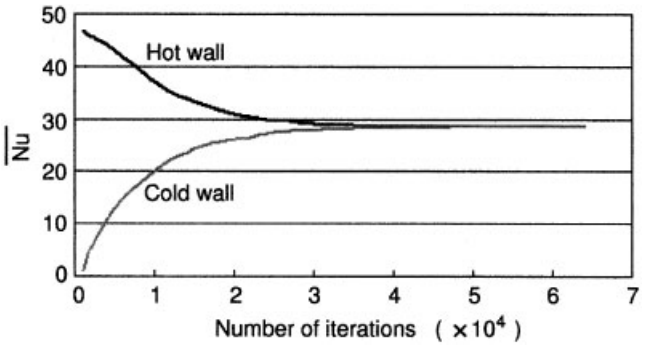

Figure 10. Convergence history of average Nusselt numbers at $Ra = 10^8$ in three-dimensional natural convection problem.

the length of vectors on the x_2–x_3 and on the x_3–x_1 planes are multiplied by a scale of 5 with respect to that on the x_1–x_2 plane. In particular, it is seen that the four vortices appear near the corners in Figure 9(b) and the strength of each vortex varies as time goes on. Thus, it is found that the flow field becomes time dependent. However, as shown in Figure 10, the average Nusselt numbers on the hot and cold walls reach almost the same value at the final state in spite of the unsteady flow. Therefore, it is shown that the present scheme can maintain the conservation of energy very well even at Rayleigh number as high as 10^8.

Finally, we examine the effects of the boundary layer. According to Gill [8], the thickness $\bar{\delta}$ of the boundary layer is estimated as $\bar{\delta} = 1.8Ra^{-1/4}$; it follows that the layer contains two nodes in the present computations. Further investigations should be made using finer meshes.

4. CONCLUDING REMARKS

The GMSR-method is proposed as a finite element fluid analysis algorithm for arbitrarily deformed elements using the error analysis approach. The GMSR-method is based on the 'generalized' MGM for a convection–diffusion equation and the SIMPLER-approach. This 'generalized' MGM is developed theoretically in the case of arbitrarily deformed elements using the error analysis approach. Thus, in the GMSR-method, since the inertia term and the pressure term are considered explicitly, only symmetrical matrices appear. Hence, it helps us reduce computational memory and computation time. Moreover, artificial viscosity and diffusivity are introduced through an error analysis approach to improve the accuracy and stability. Natural convection problems in a cavity were simulated using this GMSR-method to check the accuracy.

In the two-dimensional problem, the validity of this method is demonstrated by comparison with other numerical results. In the three-dimensional problem, at $Ra = 10^8$ the flow becomes time dependent; nevertheless the converged average Nusselt numbers on the hot and cold walls are obtained. Therefore, it is found that the GMSR-scheme with arbitrarily deformed elements can maintain the conservation of energy even at high Rayleigh numbers. Finally, it should be noted that the main advantages of the GMSR-method are considered less computational memory and shorter computation time maintaining the numerical stability.

Further investigation will be required for a total computational performance of the GMSR-method in the future.

APPENDIX A: EXPRESSIONS OF Q_i

In Figure 1, the expressions of Q_i $(i=1,2,K,8)$ at the node L are given as follows:

$$Q_1 = \sum_{K=1}^{27} P_K \cos(\alpha_{\delta K}\beta_\delta h_\delta) \tag{A1}$$

$$Q_2 = \sum_{K=1}^{27} [-(1-\phi) r_\delta D_{\delta,K}] \cos(\alpha_{\delta K}\beta_\delta h_\delta) \tag{A2}$$

$$Q_3 = \sum_{K=1}^{27} (-b_\delta F_{\delta,K}) \cos(\alpha_{\delta K}\beta_\delta h_\delta) \tag{A3}$$

$$Q_4 = \sum_{K=1}^{27} P_K \sin(\alpha_{\delta K}\beta_\delta h_\delta) \tag{A4}$$

$$Q_5 = \sum_{K=1}^{27} [-(1-\phi) r_\delta D_{\delta,K}] \sin(\alpha_{\delta K}\beta_\delta h_\delta) \tag{A5}$$

$$Q_6 = \sum_{K=1}^{27} (-b_\delta F_{\delta,K}) \sin(\alpha_{\delta K}\beta_\delta h_\delta) \tag{A6}$$

$$Q_7 = \sum_{K=1}^{27} (\phi r_\delta D_{\delta,K}) \cos(\alpha_{\delta K}\beta_\delta h_\delta) \tag{A7}$$

$$Q_8 = \sum_{K=1}^{27} (\phi r_\delta D_{\delta,K}) \sin(\alpha_{\delta K}\beta_\delta h_\delta) \tag{A8}$$

where

$$P_K = \left[\sum_{e=1}^{M} \int_{V_e} N_i N_j \, \mathrm{d}x_1 \, \mathrm{d}x_2 \, \mathrm{d}x_3 \right]_K \tag{A9}$$

$$D_{\gamma,K} = \left[\sum_{e=1}^{M} \int_{V_e} h_\gamma^2 \frac{\partial N_i}{\partial x_\gamma} \frac{\partial N_j}{\partial x_\gamma} \, \mathrm{d}x_1 \, \mathrm{d}x_2 \, \mathrm{d}x_3 \right]_K \tag{A10}$$

$$F_{\gamma,K} = \left[\sum_{e=1}^{M} \int_{V_e} h_\gamma N_i \frac{\partial N_j}{\partial x_\gamma} \, \mathrm{d}x_1 \, \mathrm{d}x_2 \, \mathrm{d}x_3 \right]_K \tag{A11}$$

for $\gamma = 1,2,3$. It should be noted that the summation convention is used for the subscript δ $(\delta = 1,2,3)$ in the above equations.

APPENDIX B: LIMIT VALUES OF Q_i, R_i AND THEIR DERIVATIVES

It should be noted that $\beta_\gamma h_\gamma \to 0$ for all $\gamma = 1,2,3$ indicates $\chi \to 0$ where $\beta_1 h_1 = \beta_2 h_2 = \beta_3 h_3 = \chi$. Also, the symbols '$\prime$' and '$\prime\prime$' denote the first and second derivatives, respectively.

(a) *Limit values of Q_i and R_i*:

$$\lim_{\beta_\gamma h_\gamma \to 0} Q_1 = \sum_{K=1}^{27} P_K \tag{B1}$$

$$\lim_{\beta_\gamma h_\gamma \to 0} Q_2 = -(1-\phi) \sum_{K=1}^{27} (r_1 D_{1,K} + r_2 D_{2,K} + r_3 D_{3,K}) \tag{B2}$$

$$\lim_{\beta_\gamma h_\gamma \to 0} Q_3 = -\sum_{K=1}^{27} (b_1 F_{1,K} + b_2 F_{2,K} + b_3 F_{3,K}) \tag{B3}$$

$$\lim_{\beta_\gamma h_\gamma \to 0} Q_7 = \phi \sum_{K=1}^{27} (r_1 D_{1,K} + r_2 D_{2,K} + r_3 D_{3,K}) \tag{B4}$$

$$\lim_{\beta_\gamma h_\gamma \to 0} Q_4 = \lim_{\beta_\gamma h_\gamma \to 0} Q_5 = \lim_{\beta_\gamma h_\gamma \to 0} Q_6 = \lim_{\beta_\gamma h_\gamma \to 0} Q_8 = 0 \tag{B5}$$

$$\lim_{\beta_\gamma h_\gamma \to 0} R_1 = \lim_{\beta_\gamma h_\gamma \to 0} \{\exp[-(\beta_\delta h_\delta)^2 r_\delta] \cos(b_\delta \beta_\delta h_\delta)\} = 1 \tag{B6}$$

$$\lim_{\beta_\gamma h_\gamma \to 0} R_2 = \lim_{\beta_\gamma h_\gamma \to 0} \{-\exp[-(\beta_\delta h_\delta)^2 r_\delta] \sin(b_\delta \beta_\delta h_\delta)\} = 0 \tag{B7}$$

(b) *Limit values of Q_i' and R_i'*

$$\lim_{\beta_\gamma h_\gamma \to 0} Q_4' = \sum_{K=1}^{27} P_K(\alpha_{1K} + \alpha_{2K} + \alpha_{3K}) \tag{B8}$$

$$\lim_{\beta_\gamma h_\gamma \to 0} Q_5' = -(1-\phi) \sum_{K=1}^{27} (r_1 D_{1,K} + r_2 D_{2,K} + r_3 D_{3,K})(\alpha_{1K} + \alpha_{2K} + \alpha_{3K}) \tag{B9}$$

$$\lim_{\beta_\gamma h_\gamma \to 0} Q_6' = -\sum_{K=1}^{27} (b_1 F_{1,K} + b_2 F_{2,K} + b_3 F_{3,K})(\alpha_{1K} + \alpha_{2K} + \alpha_{3K}) \tag{B10}$$

$$\lim_{\beta_\gamma h_\gamma \to 0} Q_8' = \phi \sum_{K=1}^{27} (r_1 D_{1,K} + r_2 D_{2,K} + r_3 D_{3,K})(\alpha_{1K} + \alpha_{2K} + \alpha_{3K}) \tag{B11}$$

$$\lim_{\beta_\gamma h_\gamma \to 0} Q_1' = \lim_{\beta_\gamma h_\gamma \to 0} Q_2' = \lim_{\beta_\gamma h_\gamma \to 0} Q_3' = \lim_{\beta_\gamma h_\gamma \to 0} Q_7' = 0 \tag{B12}$$

$$\lim_{\beta_\gamma h_\gamma \to 0} R_1' = 0 \tag{B13}$$

$$\lim_{\beta_\gamma h_\gamma \to 0} R_2' = -(b_1 + b_2 + b_3) \tag{B14}$$

(c) *Limit values of* Q_i'' *and* R_i'':

$$\lim_{\beta_\gamma h_\gamma \to 0} Q_1'' = -\sum_{K=1}^{27} P_K(\alpha_{1K} + \alpha_{2K} + \alpha_{3K})^2 \tag{B15}$$

$$\lim_{\beta_\gamma h_\gamma \to 0} Q_2'' = -(1-\phi) \sum_{K=1}^{27} (r_1 D_{1,K} + r_2 D_{2,K} + r_3 D_{3,K})(\alpha_{1K} + \alpha_{2K} + \alpha_{3K})^2 \tag{B16}$$

$$\lim_{\beta_\gamma h_\gamma \to 0} Q_3'' = \sum_{K=1}^{27} (b_1 F_{1,K} + b_2 F_{2,K} + b_3 F_{3,K})(\alpha_{1K} + \alpha_{2K} + \alpha_{3K})^2 \tag{B17}$$

$$\lim_{\beta_\gamma h_\gamma \to 0} Q_7'' = -\phi \sum_{K=1}^{27} (r_1 D_{1,K} + r_2 D_{2,K} + r_3 D_{3,K})(\alpha_{1K} + \alpha_{2K} + \alpha_{3K})^2 \tag{B18}$$

$$\lim_{\beta_\gamma h_\gamma \to 0} Q_4'' = \lim_{\beta_\gamma h_\gamma \to 0} Q_5'' = \lim_{\beta_\gamma h_\gamma \to 0} Q_6'' = \lim_{\beta_\gamma h_\gamma \to 0} Q_8'' = 0 \tag{B19}$$

$$\lim_{\beta_\gamma h_\gamma \to 0} R_1'' = -2(r_1 + r_2 + r_3) - (b_1 + b_2 + b_3)^2 \tag{B20}$$

$$\lim_{\beta_\gamma h_\gamma \to 0} R_2'' = 0 \tag{B21}$$

ACKNOWLEDGEMENTS

The authors express their thanks to Messrs. N. Hirakoso and K. Naitoh for their contributions in preliminary formulations and computations.

REFERENCES

1. Matsuda Y, Shao C, Matsumoto K, Fujita H, Ichikawa I. Finite element error analysis for three-dimensional incompressible viscous fluid flow analysis. *International Journal of Computational Fluid Dynamics* 1999; **12**:323–330.
2. Patankar SV. *Numerical Heat Transfer and Fluid Flow*. McGraw-Hill: New York, 1980.

3. Shao C, Matsuda M, Okochi S. Accuracy evaluation of the deformed elements in finite-element solution of the three-dimensional convection–diffusion equation. *Transactions of the Japan Society of Mechanical Engineers* 1997; **B63**:444–451 (in Japanese).
4. Matsuda Y, Shao C. Modified Galerkin method for unsteady two-dimensional viscous fluid flow analysis. *Journal of Computational Fluid Dynamics* 1998; **9**:293–301.
5. Matsuda Y, Shao C, Yamazaki I, Hoshihara M. Finite element analysis of unsteady natural convection. *International Journal of Computational Fluid Dynamics* 2001; **15**:19–32.
6. Hortmann M, Peric M, Scheuerer G. Finite volume multigrid prediction of laminar natural convection: Bench–Mark solutions. *International Journal for Numerical Methods in Fluids* 1990; **11**:189–207.
7. Okanaga H, Tanahashi T. Numerical analysis of natural convection in a square cavity at high Rayleigh numbers using the GSMAC finite-element method. *Transactions of the Japan Society of Mechanical Engineers* 1990; **B56**:2922–2929 (in Japanese).
8. Gill AE. The boundary-layer regime for convection in a rectangular cavity. *Journal of Fluid Mechanics* 1966; **26**:515–536.

